Short Article

Molecular Cell

Single-Molecule Analysis of the Target Cleavage Reaction by the *Drosophila* RNAi Enzyme Complex

Graphical Abstract

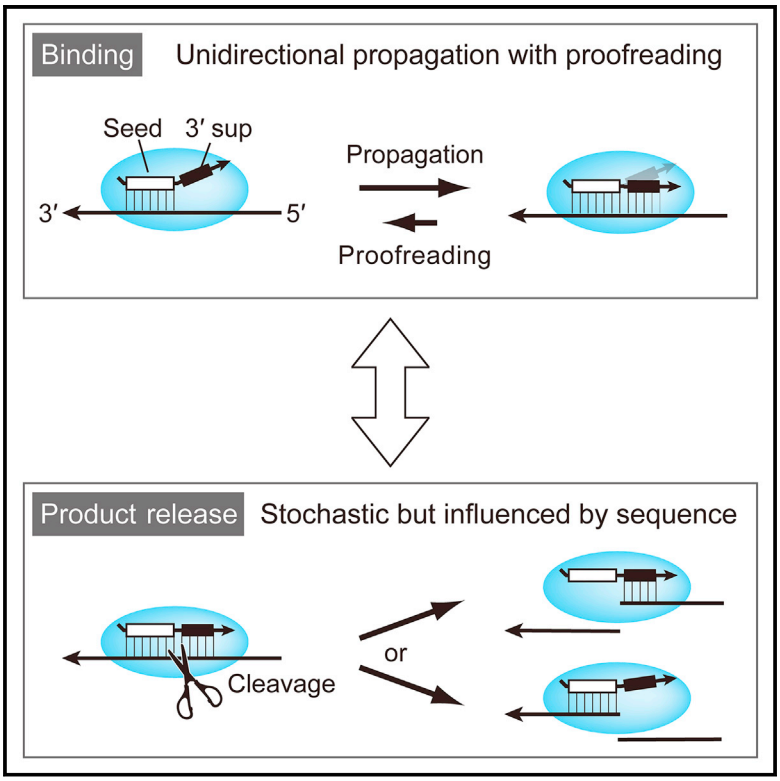

Authors

Chunyan Yao, Hiroshi M. Sasaki, Takuya Ueda, Yukihide Tomari, Hisashi Tadakuma

Correspondence

tomari@iam.u-tokyo.ac.jp (Y.T.), tadakuma.hisashi.8s@kyoto-u.ac.jp (H.T.)

In Brief

The RNA-induced silencing complex (RISC) mediates target cleavage in RNAi. Yao et al. show, by single-molecule imaging, that *Drosophila* Ago2-RISC releases the cleavage fragments, with the order influenced by the stability in each region, contrary to the unidirectional base-pairing propagation from the seed to the 3′ supplementary region upon target recognition.

Highlights

- The RNAi-mediated target cleavage reaction was analyzed by single-molecule imaging
- The seed base paring is disproportionally stabilized throughout the reaction
- Target recognition proceeds via 5′ → 3′ base-pairing propagation with proofreading
- Cleaved fragments are released independently based on the sequence and stability

Yao et al., 2015, Molecular Cell *59*, 125–132
July 2, 2015
http://dx.doi.org/10.1016/j.molcel.2015.05.015

Molecular Cell
Short Article

Single-Molecule Analysis of the Target Cleavage Reaction by the *Drosophila* RNAi Enzyme Complex

Chunyan Yao,[1,2] Hiroshi M. Sasaki,[3] Takuya Ueda,[1] Yukihide Tomari,[1,3,*] and Hisashi Tadakuma[1,4,*]
[1]Graduate School of Frontier Science, The University of Tokyo, Chiba 277-8562, Japan
[2]Department of Laboratory Medicine, Southwest Hospital, Third Military Medical University, Chongqing 400038, China
[3]Institute of Molecular and Cellular Biosciences, The University of Tokyo, Tokyo 113-0032, Japan
[4]Institute for Integrated Cell-Material Sciences, Kyoto University, Kyoto 606-8501, Japan
*Correspondence: tomari@iam.u-tokyo.ac.jp (Y.T.), tadakuma.hisashi.8s@kyoto-u.ac.jp (H.T.)
http://dx.doi.org/10.1016/j.molcel.2015.05.015

SUMMARY

Small interfering RNAs (siRNAs) direct cleavage of complementary target RNAs via an RNA-induced silencing complex (RISC) that contains Argonatute2 protein at its core. However, what happens after target cleavage remains unclear. Here we analyzed the cleavage reaction by *Drosophila* Argonaute2-RISC using single-molecule imaging and revealed a series of intermediate states in target recognition, cleavage, and product release. Our data suggest that, after cleavage, RISC generally releases the 5′ cleavage fragment from the guide 3′ supplementary region first and then the 3′ fragment from the seed region, highlighting the reinforcement of the seed pairing in RISC. However, this order can be reversed by extreme stabilization of the 3′ supplementary region or mismatches in the seed region. Therefore, the release order of the two cleavage fragments is influenced by the stability in each region, in contrast to the unidirectional base pairing propagation from the seed to the 3′ supplementary region upon target recognition.

INTRODUCTION

20- to 30-nt small RNAs guide Argonaute (Ago) family proteins, the core component of the RNA-induced silencing complex (RISC), to their target RNAs through base pairing and mediate various types of gene silencing. Previous biochemical, structural, and computational studies indicate that, in RISC, Ago proteins divide the guide strand into multiple domains with distinct properties. Among them, the seed region (guide positions 2–7 or 2–8) plays a conserved and central role in target RNA recognition (Lai, 2002; Lewis et al., 2003; Doench and Sharp, 2004; Haley and Zamore, 2004; Brennecke et al., 2005; Krek et al., 2005; Lewis et al., 2005; Ma et al., 2005; Parker et al., 2005; Grimson et al., 2007; Wang et al., 2008a, 2008b, 2009; Parker et al., 2009; Elkayam et al., 2012; Nakanishi et al., 2012; Schirle and MacRae, 2012; Wee et al., 2012; Schirle et al., 2014). Ago proteins arrange the seed region of the guide strand in an ordered, quasi-helical geometry that prepays the entropic penalty and creates an optimal site for target RNA binding (Ma et al., 2005; Parker et al., 2005, 2009; Wang et al., 2008a, 2008b, 2009; Elkayam et al., 2012; Nakanishi et al., 2012; Schirle and MacRae, 2012; Schirle et al., 2014). Mouse Ago2 and other mammalian Ago proteins, which mainly act in the microRNA-mediated repression of imperfectly complementary target mRNAs without cleavage, rely mostly on base pairs in the seed region for target recognition, with only a modest contribution from base pairs in the 3′ supplementary region (guide positions 13–16) or regions outside of the seed (Lewis et al., 2003, 2005; Doench and Sharp, 2004; Krek et al., 2005; Grimson et al., 2007; Wee et al., 2012). Indeed, mouse Ago2-RISC shows no substantial difference in the affinity between a seed-matching target and a fully complementary target (Wee et al., 2012).

In contrast, other Ago family proteins that act in target cleavage require more extensive base pairing between the guide strand and the target RNAs. For example, *Drosophila* Ago2, which is crucial for antiviral immunity via RNAi in flies, uses not only the seed region of the guide small interfering RNAs (siRNAs) but also the 3′ supplementary region and its adjacent nucleotides (guide positions 12–17, extended 3′ supplementary region) for target binding (Haley and Zamore, 2004; Wee et al., 2012). Dinucleotide mismatches at positions 4 and 5 in the seed region reduce the guide-target affinity ~600-fold, whereas mismatches at positions 15 and 16 in the extended 3′ supplementary region also weaken the affinity ~250-fold (Wee et al., 2012). Similarly, plant microRNAs loaded in AGO1 require base pairing in both the seed and the extended 3′ supplementary regions to recognize their target RNAs (Iwakawa and Tomari, 2013). However, those two regions are not functionally equivalent, but they bind to the target in a sequential manner. Biochemical evidence suggests that fly Ago2-RISC rapidly searches seed-matching sites first and then slowly propagates base pairs through the central and extended 3′ supplementary regions to fully complementary sites (Wee et al., 2012), which is accompanied by conformational rearrangement of the guide strand and Ago2 (Wang et al., 2008a, 2009; Schirle et al., 2014; Sheng et al., 2014). Only this propagated conformation with extensive base pairing allows target cleavage by RISC, preventing it from promiscuously cleaving partially matched "off targets" (Wang et al., 2009; Wee et al., 2012; Schirle et al., 2014; Sheng et al., 2014). Cleavage occurs

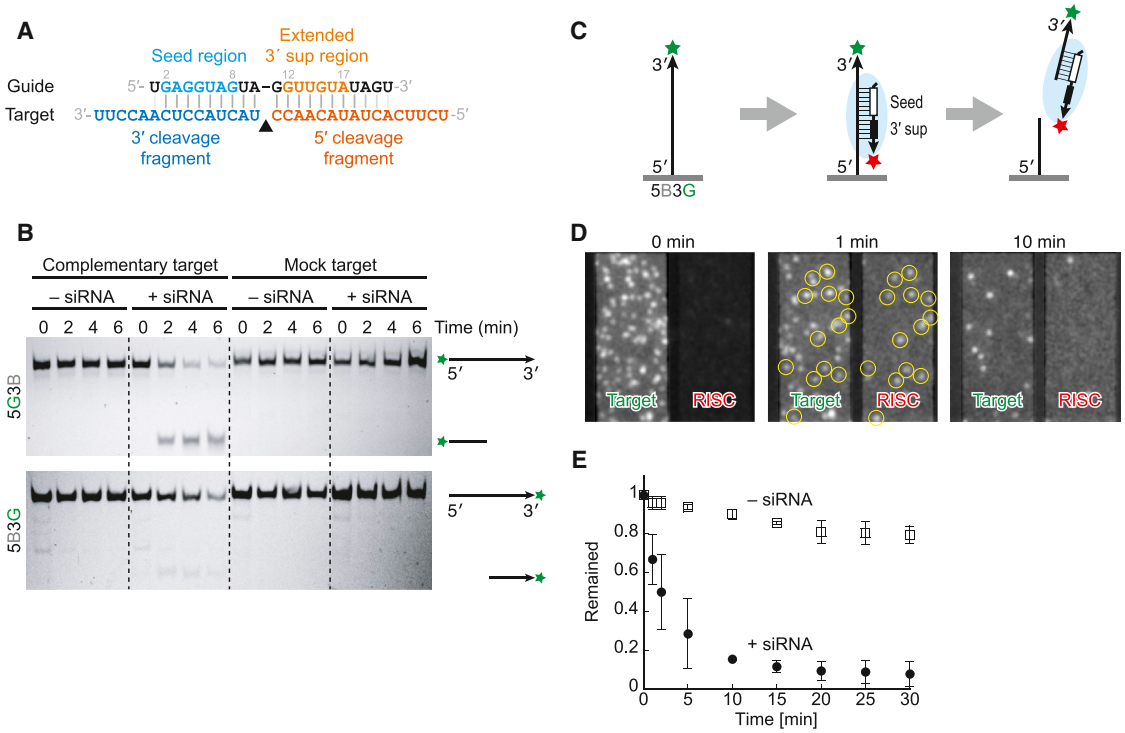

Figure 1. Cleavage of Fluorescently Labeled Target RNAs

(A) The seed region and the extended 3′ supplementary region in the *let-7* guide strand and the corresponding 3′ and 5′ cleavage fragments of the target RNA.

(B) Sequence-specific cleavage of fluorescently labeled target RNAs in bulk. The mock target was complementary to a different siRNA (luc siRNA, shown in Figure S3D).

(C) Schematic representation of surface tethering and target cleavage. 3′ sup, 3′ supplementary region.

(D) Time-lapse single-molecule images of target cleavage. Yellow circles denote co-localization of the green 5B3G target and the red RISC. See also Figure S1.

(E) Quantification of the time-lapse single-molecule experiment. The number of the green target spots decreased rapidly in the presence of the cognate siRNA-programmed RISC. Error bars indicate the SD of three independent experiments.

precisely at the phosphodiester bond between the target nucleotides across from positions 10 and 11 of the siRNA guide strand (Elbashir et al., 2001), mediated by the conserved catalytic tetrad in Ago proteins adopting the RNase H-like fold (called "slicer" activity) (Nakanishi et al., 2012). PIWI subclass proteins of the Ago family, which load PIWI-interacting RNAs (piRNAs) and protect the germline genome against transposons, also have the slicer activity and require extensive complementarity for target cleavage (Nishida et al., 2007; Reuter et al., 2011; Wang et al., 2014).

Despite advances in understanding the mechanism of target recognition and endonucleolytic cleavage by RISC, what happens after target cleavage remains unclear. RISC-mediated cleavage produces two target fragments: the 3′ cleavage fragment facing the seed region of the guide and the 5′ cleavage fragment facing the extended 3′ supplementary region of the guide (Figure 1A). Given the similar contributions of the seed region and the extended 3′ supplementary region to the overall target binding affinity for fly Ago2-RISC and plant AGO1-RISC, the two cleavage fragments may be released independently at comparable rates. Alternatively, analogous to the consecutive propagation of base pairing from the seed region to the extended 3′ supplementary region upon target binding, release of the two cleaved target fragment may also follow a unidirectional path. Intriguingly, in the "ping-pong" amplification loop for piRNA biogenesis, secondary piRNAs are generated from the 3′ fragment but not from the 5′ fragment of the cleavage product by primary piRNAs (Brennecke et al., 2007; Gunawardane et al., 2007), whereas, in plants, microRNA-mediated cleavage of long non-coding RNAs from TAS loci triggers the generation of *trans*-acting siRNAs (tasiRNAs) using either the 3′ or 5′ cleavage fragment but not from both fragments (Fei et al., 2013). Therefore, how the cleaved RNA fragments are released from RISC may impact their downstream functions. Here we utilized single-molecule imaging to analyze the target cleavage reaction by fly Ago2-RISC. Our results revealed a series of intermediate states in target recognition, cleavage, and product release by RISC and refine the molecular mechanism of RNAi in flies.

RESULTS AND DISCUSSION

Fluorescently Labeled RISC and Target RNA Are Functional for the Cleavage Reaction

To begin our single-molecule analysis of target cleavage, we sought to fluorescently label Ago2-RISC and the target RNA with two different colors. To this end, lysate from *Drosophila*

S2 cells was incubated with an siRNA duplex having a red fluorophore (Cy5) at the 3′ end of the guide strand. We also labeled either the 5′ or 3′ end of a 31-nt perfectly complementary target RNA with a green fluorophore (Alexa 555) and the other end with biotin, resulting in two kinds of targets: 5′ green fluorophore and 3′ biotin (hereafter called "5G3B") or 5′ biotin and 3′ green fluorophore (hereafter called "5B3G"). We confirmed, by bulk biochemical analysis, that Ago2-RISC programmed with the 3′ red-labeled guide strand ("red RISC") could cleave the 5G3B and 5B3G target RNAs in a sequence-specific manner (Figure 1B). Target cleavage required perfect complementarity between the guide strand and the target RNA.

To elucidate the cleavage process by Ago2-RISC at the single-molecule level, we first tethered the 5B3G target RNA to a NeutrAvidin-derived quartz glass surface (Figure 1C). The tethered 5B3G target was observed as green fluorescent spots by simultaneous irradiation with a green laser (514 nm) and a red laser (633 nm) (Figure 1D, left). After infusion of the red RISC onto the glass surface, we observed red fluorescent spots that co-localized with a part of the green spots (Figure 1D, center). The fluorescence intensity of the observed green and red spots was the same as that of a single fluorophore (Figures S1A and S1B). After 10-min incubation, both green and red spots largely disappeared (Figure 1D, right). A time-lapse experiment (10-s data acquisition at each time point) revealed that the number of 5B3G target spots decreased rapidly in the presence of the cognate red RISC but not in its absence (Figure 1E). The target spot number remained largely unchanged when cleavage was blocked by the introduction of central mismatches at positions 10-11 (Figure S1C). Taken together, we concluded that the observed green and red spots represent single 5B3G target and red RISC, respectively, and that the disappearance of the green spots reflects the target cleavage process by RISC.

The 5′ Cleavage Fragment Is First Released from the Extended 3′ Supplementary Region of the Guide

There are two possible scenarios for the release of the cleaved target: the 3′ cleavage fragment facing the seed region of RISC is released first, or the 5′ cleavage fragment facing the extended 3′ supplementary region of RISC is released first (Figure 2A). To address this question, we next continuously monitored the appearance and disappearance of the spots during incubation using the 5B3G or 5G3B target RNA and the red RISC. For continuous single-molecule imaging, the photobleaching effect can be a concern. To avoid this, we first determined the photobleaching rate by fixing a non-cleavable 2′ *O*-methylated green target on the glass surface with the red RISC infused and continuously exciting the green target and red RISC (Figure S1D). The actual observation condition was then set to minimize the photobleaching effect without compromising the signal-to-noise ratio and the time resolution (Figure S1E).

In our continuous observation of the red RISC and the 5B3G target, the red spots of RISC appeared on the green spot, reflecting target recognition by RISC (Figure 2B). The red spots stayed there for ~20 s and then disappeared (Figure 2B; Figure S2). In addition, we observed the disappearance of the green spot after co-localization with the red spot (Figure 2B), which should represent RISC-mediated target cleavage and the release of the non-anchored 3′ fragment of the 5B3G target. We gathered these active RISC interaction events and measured the lag time between the disappearance of the green spot and that of the red spot. If the seed region of RISC first releases the 3′ cleavage fragment of the 5B3G target, then there should be a lag time after the disappearance of the green spots before that of the red spots (Figure 2A, seed release first). On the other hand, if the extended 3′ supplementary region of RISC first releases the 5′ cleavage fragment, then no lag time should be observed (Figure 2A, 3′ supplementary release first). Our analysis of continuous imaging revealed that ~80% of the green fluorophore at the 3′ end of the 5B3G target disappeared simultaneously with the red fluorophore on RISC (Figure 2C). The same was true when the red and green colors were reversed (Cy3 at the 3′ end of the guide strand [the green RISC] and the red dye ATTO 647N at the 3′ end of the target [the 5B3R target]; see also Figures 3B and 3E, wild-type [WT]). Therefore, RISC tends to first release the 5′ cleavage fragment facing the extended 3′ supplementary region.

To confirm the order of cleaved target release, we reversed the direction of target anchoring, tethering the 3′ end of the target on the glass surface via biotin and attaching the green dye at the 5′ end of the target (5G3B, Figure 2D). If RISC stays bound to the anchored 3′ cleavage fragment via the seed region, then there should be a lag time between the disappearance of the non-anchored 5′ end of the target and that of RISC. We note that, when the red RISC binds to the 5G3B target, two fluorescent dyes (Alexa 555 at the 5′ end of the target and Cy5 at the 3′ end of the guide strand) locate in close proximity (Figure 2D). Therefore, strong fluorescence resonance energy transfer (FRET) from the target's green florescent dye to the RISC's red florescent dye is expected, which should suppress the target's green signal and increase RISC's red signal. If RISC first releases the 5′ cleavage fragment from the extended 3′ supplementary region of the guide, then FRET is abolished, and the red signal of RISC should be decreased (Figure 2D). Supporting this model, the expected traces of red and green spots were observed in our continuous monitoring of the red RISC and the 5G3B target (Figure 2D). Importantly, there was a clear lag between the termination of FRET (decrease of the red signal) and the disappearance of the red spots (Figure 2D), which was observed in ~70% of the target (Figure 2E). The time constant (τ) for the lag time was ~10 s (Figure 2E), and a similar value was obtained when the two colors were reversed (Cy3 at the 3′ end of the guide strand [the green RISC] and the red dye ATTO 647N at the 5′ end of the target [the 5R3B target]; see also Figures S3A and S3C, WT). These data strongly support the model proposing that RISC first releases the 5′ cleavage fragment from the extended 3′ supplementary region of the guide strand.

The Strength of the Guide-Target Base Pairing Influences the Release Order of the Cleaved Target Fragments

Our finding that RISC first releases the 5′ cleaved target fragment from the extended 3′ supplementary region and keeps the 3′ cleavage fragment paired with the seed region longer (Figure 2) suggests that the seed pairing is more stable than the extended 3′ supplementary pairing after target cleavage, which may

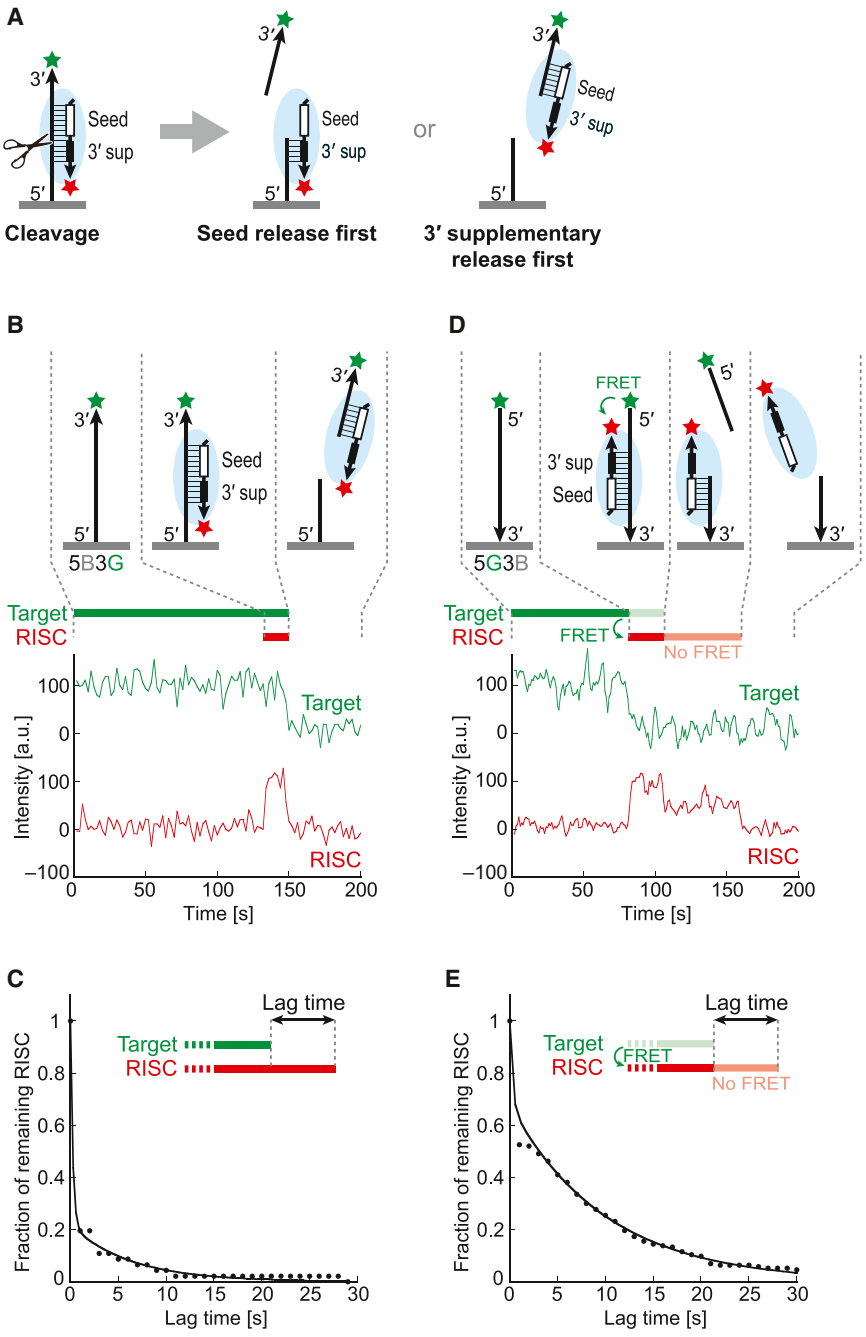

Figure 2. The Seed Region Releases the Cleaved Target Fragment before the Extended 3′ Supplementary Region

(A) Schematic representation of the two possible scenarios after target cleavage.

(B) Representative continuous single-molecule observation for the cleavage of the 5B3G target. a.u., arbitrary unit. See also Figure S2.

(C) Plot of the lag time after the disappearance of the green spots before the disappearance of the red spots. Approximately 80% of the green spots showed a simultaneous disappearance with the red spots, indicating the prior release of the 5′ cleavage fragment from the extended 3′ supplementary region.

(D) Representative continuous single-molecule observation for the cleavage of the 5G3B target. Note that strong FRET occurs in the experimental setting.

(E) Plot of the lag time after the loss of FRET (i.e., the disappearance of the proximal green fluorophore) before the disappearance of the red spots. Approximately 70% of the green spots showed a delayed disappearance of the red spots after the loss of FRET, indicating the prior release of the 5′ cleavage fragment from the extended 3′ supplementary region.

represent disproportional stabilization of the seed pairing in the post-cleavage conformation of Ago2-RISC. However, the sequence of the siRNA guide strand we used so far contains more G/Cs in the seed region than in the extended 3′ supplementary region. Accordingly, even in the absence of Ago protein, the base pair hybridization between the 21-nt guide strand and the 15-nt 3′ cleavage fragment (facing the seed region, ΔG = –15.3 kcal/mol [no Ago contribution considered for ΔG calculation, similarly hereafter]) is more stable than that between the guide stand and the 16-nt 5′ cleavage fragment (facing the extended 3′ supplemental region, ΔG = –14.7 kcal/mol) (Figure 3A, WT), which may simply explain the ordered release of the cleaved target fragments.

To elucidate the contribution of the base pairing stability to the order of cleaved target release, we examined the target cleavage process with more G-C pairs introduced between the guide strand and the target RNA to stabilize the seed region or the extended 3′ supplementary region. We designed three additional siRNA-target pairs: 5GC (the 5′ seed region is stabilized, ΔG = –20.3 kcal/mol for the guide strand and the 3′ cleavage fragment), 3GC (the extended 3′ supplementary region is stabilized, ΔG = –18.6 kcal/mol for the guide strand and the 5′ cleavage fragment), and 3GC2 (the extended 3′ supplementary region is stabilized further, ΔG = –22.8 kcal/mol for the guide strand and the 5′ cleavage fragment) (Figure 3A). We labeled the 3′ end of the guide strand with green Cy3 dye (green RISC) while tethering the 5′ end of the target RNA on the glass surface and labeling the 3′ end with red ATTO 647N dye (5B3R) because this experimental setting provided a high signal-to-noise ratio over a long duration and was most suitable for comparing different sequences (note that a weak FRET is observed in this condition). We then evaluated the effect of the base-paring stabilization on the cleavage product release by single-molecule imaging (Figures 3B–3E). As shown above,

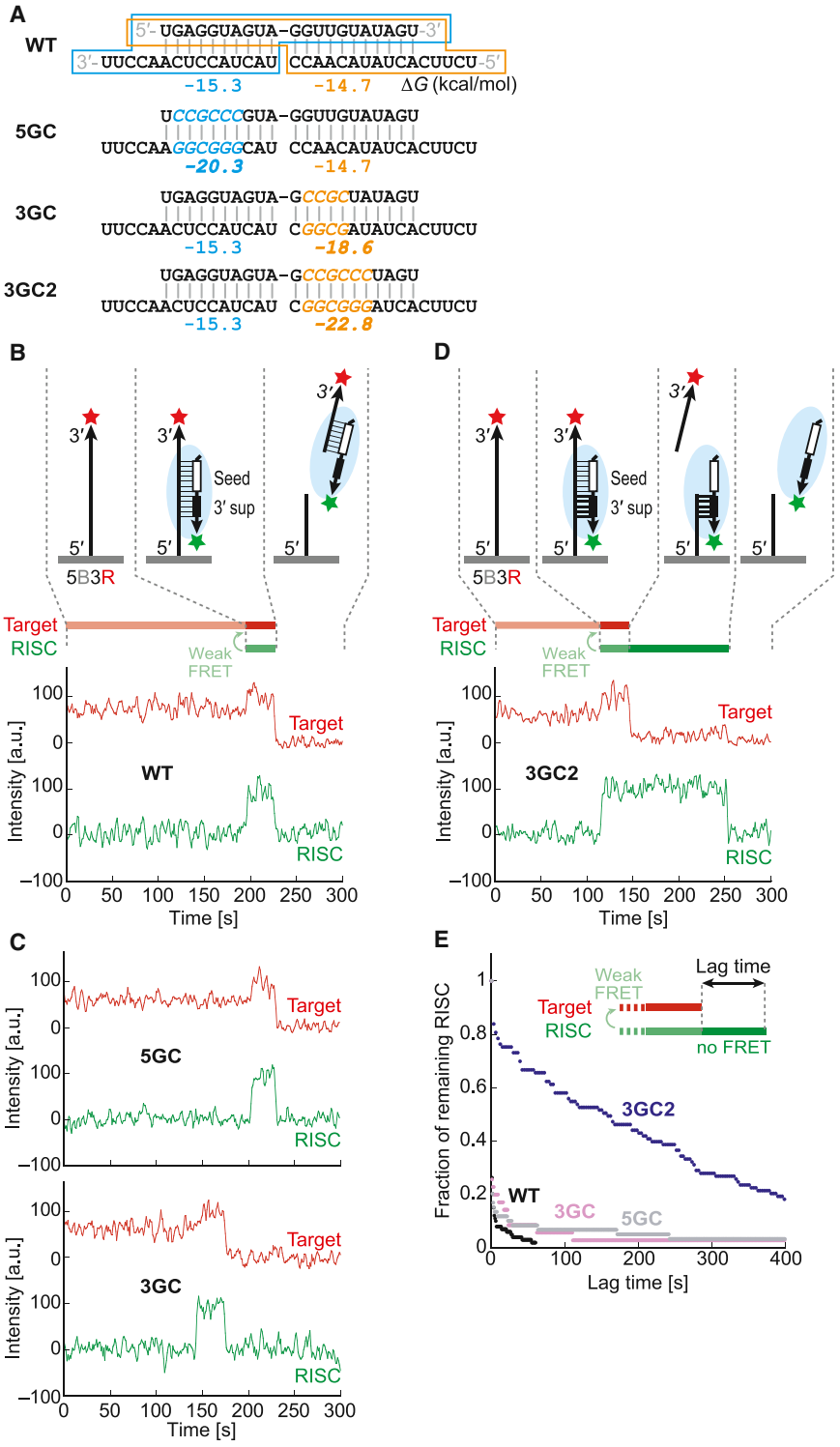

Figure 3. The Strength of the Guide-Target Base Pairing Affects the Release Order of the Cleaved Target Fragments

(A) Strengthened base pairing between the guide strand and the cleaved target fragments in the seed region or the extended 3′ supplementary region. ΔG values were calculated by using RNAduplex in the ViennaRNA package (v. 2.1.7, http://www.tbi.univie.ac.at/RNA/).

(B) Representative continuous single-molecule observation for the cleavage of the WT target. Note that weak FRET occurs in this experimental setting.

(C) Representative continuous single-molecule observation for the cleavage of the 5GC and 3GC targets. Note that weak FRET occurs in this experimental setting.

(D) Representative continuous single-molecule observation for the cleavage of the 3GC2 target. Note that weak FRET occurs in this experimental setting.

(E) Plot of the lag time after the disappearance of the red spots before the disappearance of the green spots. 3GC2 showed a delayed disappearance of the green spots after the disappearance of the red spots, indicating the prior release of the 3′ cleavage fragment from the seed region. See also Figure S3.

the wild-type sequence caused the simultaneous disappearance of the green RISC signal and the red target signal, which reflects the prior release of the 5′ cleaved target fragment from the extended 3′ supplementary region of the guide (Figures 3B and 3E, WT). This order of target release was unchanged when the seed region was stabilized (Figures 3C and 3E, 5GC). Even for 3GC, in which the modest stabilization of the extended 3′ supplementary region inverted the order of the calculated annealing affinity of the guide strand to the 3′ and 5′ cleavage fragments (ΔG = –15.3 and –18.6 kcal/mol, respectively; Figure 3A, 3GC), the extended 3′ supplementary region was still the first to release the cleavage product (Figures 3C and 3E, 3GC). This observation highlights the reinforcement of the seed base pairing by Ago protein even after target cleavage. Intriguingly, however, when the extended 3′ supplementary region was further stabilized by two additional GC pairs (ΔG = –22.8 kcal/mol for the guide strand and the 5′ cleavage fragment; Figure 3A, 3GC2), we observed a clear lag time after the disappearance of the red 3′ cleavage fragment before that of the green RISC (Figures 3D and 3E, 3GC2), indicating that the seed region was now the first to release the cleavage product. The 5′ cleavage fragment remained on the extended 3′ supplementary region for a long time, with the time constant being ~300 s (Figure 3E, 3GC2). This reversed order of the cleaved target fragment release was confirmed by switching the direction of target anchoring and labeling (5R3B, Figures S3A–S3C).

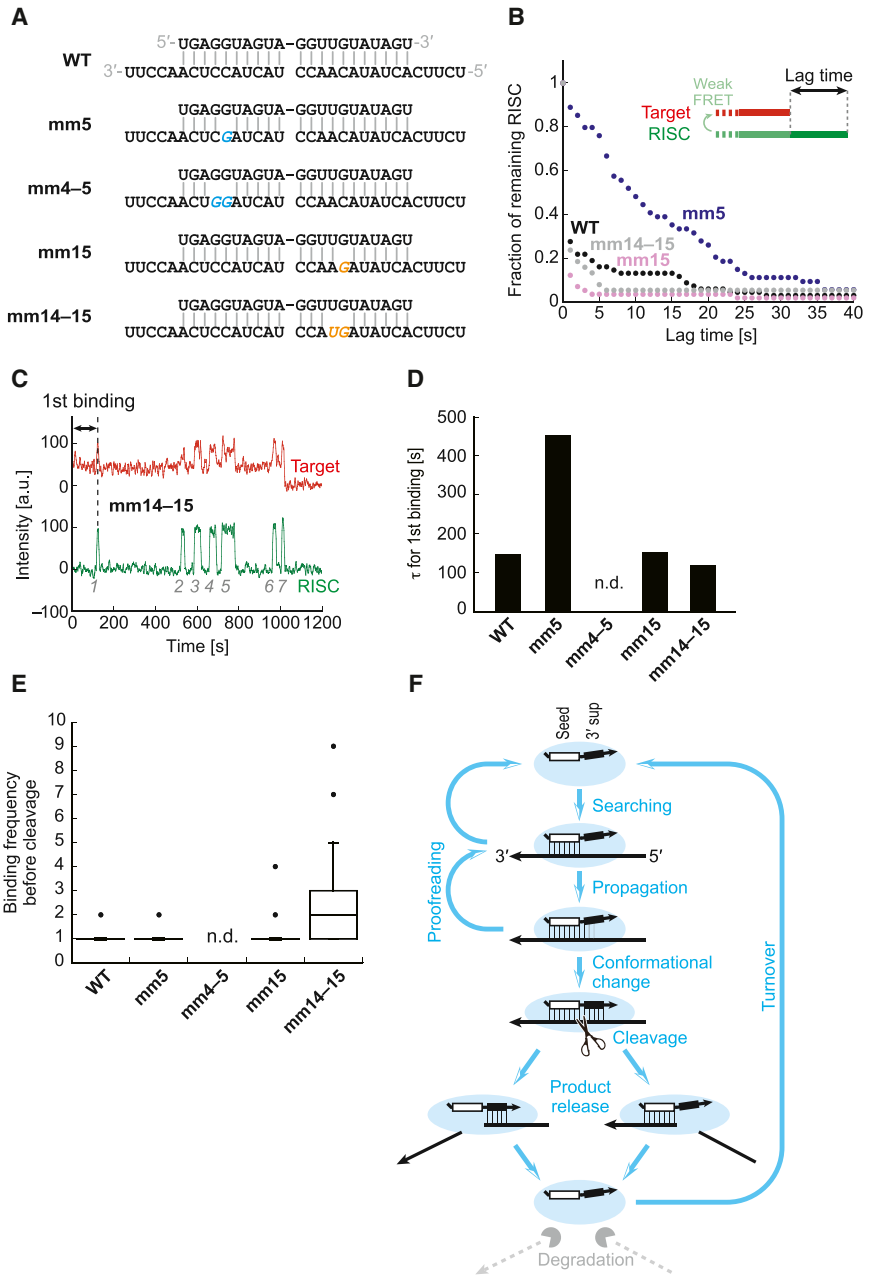

Figure 4. Target Recognition, Cleavage, and Product Release for Mismatched Targets

(A) *let-7* targets with one or two mismatch(es) in the seed region or the 3′ supplementary region.

(B) Plot of the lag time after the disappearance of the red spots before the disappearance of the green spots. mm5 with a mismatch in the seed region showed a delayed disappearance of the green spots after the disappearance of the red spots, indicating the prior release of the 3′ cleavage fragment from the seed region.

(C) Representative continuous single-molecule observation for the cleavage of the mm14-15 target. Note that weak FRET occurs in this experimental setting. The arrow indicates the time required for the first binding. Italicized numbers show the number of binding events before cleavage.

(D) Time constants (τ) for the time required for the first binding (illustrated in C), calculated from the cumulative plot (Figure S4). mm5 with a mismatch in the seed region required ~3-fold longer for initial target recognition. n.d., too long to be determined.

(E) Box plots showing the distribution of the binding event number before cleavage. WT, mm5, and mm15 required only a single binding event before cleavage, whereas mm14-15 required multiple binding events.

(F) A refined model for target recognition, cleavage, product release, and RISC turnover.

To further validate that the strength of the guide-target base pairing can change the release order of the cleaved target fragments, we introduced one or two mismatches in the *let-7* target RNA at guide position 5 (mm5) or positions 4-5 (mm4-5) in the seed region or position 15 (mm15) or positions 14-15 (mm14-15) in the 3′ supplementary region (Figure 4A). We could hardly detect target cleavage for mm4-5 with two mismatches in the seed region, precluding further analysis. As expected, mm15 and mm14-15 showed the same order of target release as the WT. The 5′ cleavage fragment was first released from the extended 3′ supplementary region of the guide strand (Figure 4B). In contrast, the order was reversed for mm5 with one mismatch in the seed region. The 3′ cleavage fragment was first released from the seed region (Figure 4B). These results suggest that, although the seed pairing is more strengthened than the extended 3′ supplementary pairing in RISC, the product release processes of the 3′ and 5′ cleavage fragments are not consecutively coupled but occur independently on the basis of the stability in each region. Indeed, another siRNA (targeting the firefly luciferase gene), whose extended 3′ supplementary pairing (ΔG = –18.2 kcal/mol for the guide strand and the 5′ cleavage fragment) is much more stable than the seed pairing (ΔG = –11.8 kcal/mol for the guide strand and the 3′ cleavage fragment), first released the 3′ cleavage fragment from the seed region (Figure S3D).

Effect of Mismatches for Target Recognition and Cleavage

Unlike the 5GC, 3GC, and 3GC2 series (Figure 3A), in which corresponding siRNA and target pairs with different sequences were used, the mm series (Figure 4A) used the same siRNA sequence for all mismatched target sequences. Therefore, we can directly compare and analyze the effect of mismatches

for target recognition and cleavage by the same RISC. We measured the time required for the first target binding in our continuous monitoring (Figures 4C and 4D). The time constant (τ) for the first binding was ~150 s for the WT, mm15, and mm14-15 (Figures 4D; Figure S4), indicating that mismatches in the 3′ supplementary region do not affect target binding. In contrast, τ was ~450 s for mm5, ~3-fold longer than that of the WT (Figure 4D; Figure S4). Therefore, target recognition by RISC depends on base pairing in the seed region but not in the 3′ supplementary region, emphasizing the importance of seed pairing for initial target recognition.

The WT, mm5, and mm15 required only a single binding event before target cleavage (Figure 4E), indicating that virtually every RISC cleaved the target before dissociating from it. Intriguingly, however, when there were two mismatches in the 3′ supplementary region (mm14-15), RISC required multiple (a median of 2 and up to 9) binding events before target cleavage (Figures 4C and 4E). Therefore, the mismatches in the 3′ supplementary region prevent RISC from reaching its cleavage-competent conformation, promoting dissociation of RISC without cleavage.

A Refined Model for the Molecular Mechanism of RNAi in Flies

Using single-molecule imaging, we here successfully detected a series of intermediate states in the target recognition, cleavage, and product release by *Drosophila* Ago2-RISC. Our current results and previous biochemical and structural findings together lead to a refined model for the molecular mechanism of RNAi in flies (Figure 4F). First, RISC searches its potential target RNAs using the seed region of the guide stand pre-arranged for base pairing by the quasi-helical geometry. Initial target recognition depends critically on base pairing in the seed region, but not in the 3′ supplementary region. When the target is recognized, RISC then extends base pairing toward the 3′ direction until extensive base pairs induce the cleavage-competent conformation. Such 5′ → 3′ base-pairing propagation is hindered in the presence of mismatches in the 3′ supplementary region, promoting the dissociation of RISC before target cleavage. This could act as a proofreading mechanism to prevent the cleavage of off-targets. After target cleavage, the seed region still remains more reinforced than the extended 3′ supplementary region, but the releases of the two cleavage fragments occur independently on the basis of the stability in each region. The released target fragments are rapidly degraded by cellular ribonucleases (Orban and Izaurralde, 2005), thereby facilitating RISC turnover. It will be interesting to apply the single-molecule imaging approach to analyze the behavior of RISC for other slicer-competent Ago proteins in the future, especially in the context of secondary piRNA and plant tasiRNA biogenesis pathways, where the 3′ and 5′ cleavage fragments play distinct functions.

EXPERIMENTAL PROCEDURES

Preparation of S2 Cell Lysate

Lysate from S2 cells was prepared by Dounce homogenization using lysis buffer (30 mM HEPES-KOH [pH 7.4], 100 mM KOAc, and 2 mM $Mg(OAc)_2$) containing 1 mM DTT and 1× complete EDTA-free protease inhibitor cocktail (Roche), as described previously (Haley et al., 2003).

Bulk Target Cleavage Assays

Preparation of 40× reaction mix (containing ATP, an ATP regeneration system, amino acids, and RNase inhibitor) and quenching of the reaction by Proteinase K treatment have been described in detail (Haley et al., 2003). Small RNAs and target RNAs were purchased from IDT or Japan Bio Services with or without chemical labeling of Cy3, Cy5, Alexa 555, ATTO 647N, or biotin at the 5′ or 3′ end. The bulk solution assay was performed with 50 nM small RNA duplex and 100 nM target RNA and analyzed by 12% 8M urea gel as described previously (Haley et al., 2003). Gel images were captured by LAS4000 (GE Healthcare).

Single-Molecule Imaging

Flow chambers in which 2.5- to 4-nM targets were anchored on polyethylene glycol (PEG)-coated quartz slides were prepared as described previously (Miyazono et al., 2010; Zhou et al., 2011), and S2 lysate containing siRNA-programmed Ago2-RISC and the O_2 scavenger system (Harada et al., 1990) was infused. Single-molecule images were visualized by a total internal reflection fluorescence microscope equipped on an inverted type microscope (IX71, Olympus) as described previously (Funatsu et al., 1995; Miyazono et al., 2010). The Cy3/Alexa 555 and Cy5/ATTO 647N dyes were illuminated with a diode-pumped solid-state (DPSS) laser (514 nm; Fantango, Cobolt) and a He-Ne laser (633 nm; GLG5410, SOC), respectively. Fluorescence images from Cy3/Alexa 555 and Cy5/ATTO 647N were separated by using a DualView (Optical Insights) and then projected side-by-side onto an electron-multiplying charge-coupled device camera (iXon DV860 DCS-BV, Andor). Images were taken at a frame rate of 0.3–1 frames/s, and the observations were carried out at 24 ± 1°C.

Data Analysis

Images were analyzed using ImageJ software (http://rsb.info.nih.gov/ij/) with a built-in function and custom-designed plug-in software. The fluorescent intensity of the spots was measured using 6-pixel-diameter circular regions of interest (ROIs). To analyze the lag time, data were fitted by non-linear least-squares to the following equation: $C1 \times \exp(-t / C2) + (1 - C1) \times \exp(-t / C3)$, where $C1$ is a normalized parameter, $C2$ is the lag time for fast components, and $C3$ is the lag time for slow components. To determine the lifetime of the fluorophore (Figure S1) and the first binding time of red RISC on mismatched targets (Figure 4D; Figure S4), data were fitted by non-linear least-squares to the following equation: $C1 \times (1 - \exp(-t / C2))$, where $C1$ is a normalized parameter, $C2$ is the lifetime of the fluorophore for Figure S1 or τ for the first binding for Figure 4D and Figure S4.

SUPPLEMENTAL INFORMATION

Supplemental Information includes four figures and can be found with this article online at http://dx.doi.org/10.1016/j.molcel.2015.05.015.

AUTHOR CONTRIBUTIONS

H.T. and Y.T. conceived, designed, and supervised the study. C.Y. and H.T. performed biochemical experiments, single-molecule imaging, and data analysis. H.M.S. prepared the lysate from S2 cells and supported biochemical experiments. T.U. supervised C.Y. All authors discussed the results. H.T. and Y.T. wrote the manuscript.

ACKNOWLEDGMENTS

We thank Kaori Kiyokawa for the maintenance and propagation of S2 cells and the members of our laboratory for discussions and critical comments on the manuscript. This work was supported in part by Grants-in-Aid for Scientific Research on Innovative Areas (“Functional machinery for non-coding RNAs” and “non-coding RNA neo-taxonomy”) (to H.T. and Y.T.), a Grant-in-Aid for Young Scientists (A) (to H.T.), a Grant-in-Aid for Challenging Exploratory

Research (to H.M.S.), a Japan-China Sasakawa Medical Fellowship from The Nippon Foundation and National Natural Science Foundation of China (81371885, to C.Y.), and a Research Award from the Takeda Science Foundation (to Y.T.).

Received: December 16, 2014
Revised: April 2, 2015
Accepted: May 4, 2015
Published: July 2, 2015

REFERENCES

Brennecke, J., Stark, A., Russell, R.B., and Cohen, S.M. (2005). Principles of microRNA-target recognition. PLoS Biol. *3*, e85.

Brennecke, J., Aravin, A.A., Stark, A., Dus, M., Kellis, M., Sachidanandam, R., and Hannon, G.J. (2007). Discrete small RNA-generating loci as master regulators of transposon activity in *Drosophila*. Cell *128*, 1089–1103.

Doench, J.G., and Sharp, P.A. (2004). Specificity of microRNA target selection in translational repression. Genes Dev. *18*, 504–511.

Elbashir, S.M., Martinez, J., Patkaniowska, A., Lendeckel, W., and Tuschl, T. (2001). Functional anatomy of siRNAs for mediating efficient RNAi in *Drosophila melanogaster* embryo lysate. EMBO J. *20*, 6877–6888.

Elkayam, E., Kuhn, C.D., Tocilj, A., Haase, A.D., Greene, E.M., Hannon, G.J., and Joshua-Tor, L. (2012). The structure of human argonaute-2 in complex with miR-20a. Cell *150*, 100–110.

Fei, Q., Xia, R., and Meyers, B.C. (2013). Phased, secondary, small interfering RNAs in posttranscriptional regulatory networks. Plant Cell *25*, 2400–2415.

Funatsu, T., Harada, Y., Tokunaga, M., Saito, K., and Yanagida, T. (1995). Imaging of single fluorescent molecules and individual ATP turnovers by single myosin molecules in aqueous solution. Nature *374*, 555–559.

Grimson, A., Farh, K.K., Johnston, W.K., Garrett-Engele, P., Lim, L.P., and Bartel, D.P. (2007). MicroRNA targeting specificity in mammals: determinants beyond seed pairing. Mol. Cell *27*, 91–105.

Gunawardane, L.S., Saito, K., Nishida, K.M., Miyoshi, K., Kawamura, Y., Nagami, T., Siomi, H., and Siomi, M.C. (2007). A slicer-mediated mechanism for repeat-associated siRNA 5′ end formation in *Drosophila*. Science *315*, 1587–1590.

Haley, B., and Zamore, P.D. (2004). Kinetic analysis of the RNAi enzyme complex. Nat. Struct. Mol. Biol. *11*, 599–606.

Haley, B., Tang, G., and Zamore, P.D. (2003). In vitro analysis of RNA interference in *Drosophila melanogaster*. Methods *30*, 330–336.

Harada, Y., Sakurada, K., Aoki, T., Thomas, D.D., and Yanagida, T. (1990). Mechanochemical coupling in actomyosin energy transduction studied by in vitro movement assay. J. Mol. Biol. *216*, 49–68.

Iwakawa, H.O., and Tomari, Y. (2013). Molecular insights into microRNA-mediated translational repression in plants. Mol. Cell *52*, 591–601.

Krek, A., Grün, D., Poy, M.N., Wolf, R., Rosenberg, L., Epstein, E.J., MacMenamin, P., da Piedade, I., Gunsalus, K.C., Stoffel, M., and Rajewsky, N. (2005). Combinatorial microRNA target predictions. Nat. Genet. *37*, 495–500.

Lai, E.C. (2002). Micro RNAs are complementary to 3′ UTR sequence motifs that mediate negative post-transcriptional regulation. Nat. Genet. *30*, 363–364.

Lewis, B.P., Shih, I.H., Jones-Rhoades, M.W., Bartel, D.P., and Burge, C.B. (2003). Prediction of mammalian microRNA targets. Cell *115*, 787–798.

Lewis, B.P., Burge, C.B., and Bartel, D.P. (2005). Conserved seed pairing, often flanked by adenosines, indicates that thousands of human genes are microRNA targets. Cell *120*, 15–20.

Ma, J.B., Yuan, Y.R., Meister, G., Pei, Y., Tuschl, T., and Patel, D.J. (2005). Structural basis for 5′-end-specific recognition of guide RNA by the *A. fulgidus* Piwi protein. Nature *434*, 666–670.

Miyazono, Y., Hayashi, M., Karagiannis, P., Harada, Y., and Tadakuma, H. (2010). Strain through the neck linker ensures processive runs: a DNA-kinesin hybrid nanomachine study. EMBO J. *29*, 93–106.

Nakanishi, K., Weinberg, D.E., Bartel, D.P., and Patel, D.J. (2012). Structure of yeast Argonaute with guide RNA. Nature *486*, 368–374.

Nishida, K.M., Saito, K., Mori, T., Kawamura, Y., Nagami-Okada, T., Inagaki, S., Siomi, H., and Siomi, M.C. (2007). Gene silencing mechanisms mediated by Aubergine piRNA complexes in *Drosophila* male gonad. RNA *13*, 1911–1922.

Orban, T.I., and Izaurralde, E. (2005). Decay of mRNAs targeted by RISC requires XRN1, the Ski complex, and the exosome. RNA *11*, 459–469.

Parker, J.S., Roe, S.M., and Barford, D. (2005). Structural insights into mRNA recognition from a PIWI domain-siRNA guide complex. Nature *434*, 663–666.

Parker, J.S., Parizotto, E.A., Wang, M., Roe, S.M., and Barford, D. (2009). Enhancement of the seed-target recognition step in RNA silencing by a PIWI/MID domain protein. Mol. Cell *33*, 204–214.

Reuter, M., Berninger, P., Chuma, S., Shah, H., Hosokawa, M., Funaya, C., Antony, C., Sachidanandam, R., and Pillai, R.S. (2011). Miwi catalysis is required for piRNA amplification-independent LINE1 transposon silencing. Nature *480*, 264–267.

Schirle, N.T., and MacRae, I.J. (2012). The crystal structure of human Argonaute2. Science *336*, 1037–1040.

Schirle, N.T., Sheu-Gruttadauria, J., and MacRae, I.J. (2014). Structural basis for microRNA targeting. Science *346*, 608–613.

Sheng, G., Zhao, H., Wang, J., Rao, Y., Tian, W., Swarts, D.C., van der Oost, J., Patel, D.J., and Wang, Y. (2014). Structure-based cleavage mechanism of *Thermus thermophilus* Argonaute DNA guide strand-mediated DNA target cleavage. Proc. Natl. Acad. Sci. USA *111*, 652–657.

Wang, Y., Juranek, S., Li, H., Sheng, G., Tuschl, T., and Patel, D.J. (2008a). Structure of an argonaute silencing complex with a seed-containing guide DNA and target RNA duplex. Nature *456*, 921–926.

Wang, Y., Sheng, G., Juranek, S., Tuschl, T., and Patel, D.J. (2008b). Structure of the guide-strand-containing argonaute silencing complex. Nature *456*, 209–213.

Wang, Y., Juranek, S., Li, H., Sheng, G., Wardle, G.S., Tuschl, T., and Patel, D.J. (2009). Nucleation, propagation and cleavage of target RNAs in Ago silencing complexes. Nature *461*, 754–761.

Wang, W., Yoshikawa, M., Han, B.W., Izumi, N., Tomari, Y., Weng, Z., and Zamore, P.D. (2014). The initial uridine of primary piRNAs does not create the tenth adenine that Is the hallmark of secondary piRNAs. Mol. Cell *56*, 708–716.

Wee, L.M., Flores-Jasso, C.F., Salomon, W.E., and Zamore, P.D. (2012). Argonaute divides its RNA guide into domains with distinct functions and RNA-binding properties. Cell *151*, 1055–1067.

Zhou, Z.P., Shimizu, Y., Tadakuma, H., Taguchi, H., Ito, K., and Ueda, T. (2011). Single molecule imaging of the trans-translation entry process via anchoring of the tagged ribosome. J. Biochem. *149*, 609–618.

Molecular Cell, Volume *59*

Supplemental Information

Single-Molecule Analysis of the Target Cleavage Reaction by the Drosophila RNAi Enzyme Complex

Chunyan Yao, Hiroshi M. Sasaki, Takuya Ueda, Yukihide Tomari, and Hisashi Tadakuma

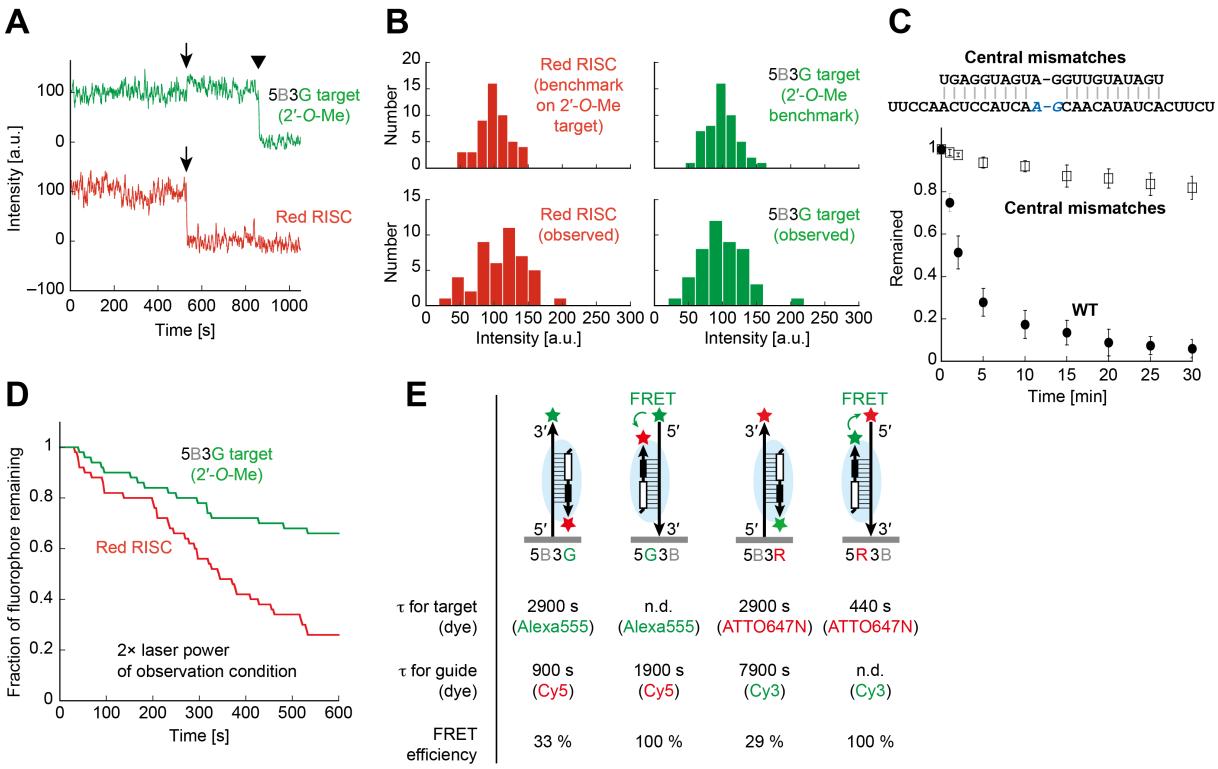

Figure S1. Observation conditions for single-molecule imaging, Related to Figure 1.

A. Upon one-step photobleaching of the Cy5 red dye on RISC (arrow), the intensity of the Alexa 555 signal on the 5B3G non-cleavable 2′-*O*-methylated target was increased (arrow), which then photobleached in one step (triangle), indicating a single RISC molecule on a single benchmark target.

B. Left, the intensity histograms of Cy5 dye on red RISC for benchmark (red RISC bound on the 5B3G non-cleavable 2′-*O*-methylated target) and for the observed signal (red RISC during cleavage of the 5B3G target) showed similar distributions, indicating that the observed red signal represents single RISC molecules. Right, the intensity histograms of Alexa 555 dye for benchmark (5B3G non-cleavable 2′-*O*-methylated target) and for the observed signal (5B3G target cleaved by the red RISC) showed similar distributions, indicating that the observed green signal represents single target molecules. Intensity of benchmark was set to 100 [a.u.].

C. Central mismatches at guide positions 10 and 11 blocked the target spots to disappear. Error bars indicate the standard deviation of three independent experiments.

D. Fluorophore survival curve for red RISC on 5B3G non-cleavable 2′-*O*-methylated target. The laser power was twice stronger than that used for the observation condition.

E. The time constant (τ) for fluorophore lifetime and FRET efficiency for the observation conditions. FRET efficiency was estimated from the trace of active RISC interaction (n = 49 and 42 for 5B3G and 5B3R, respectively). In all conditions, the photobleaching effect was small enough compared to the observed lag time and duration. n.d.: too long to be determined.

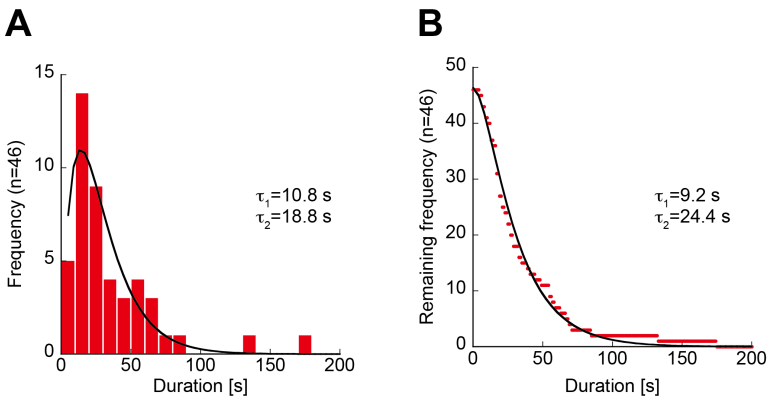

Figure S2. Duration time of RISC binding to the target RNA, Related to Figure 2.

A. The lifetime histogram of the red RISC on 5B3G target tethered on the glass surface. Data was fitted by the two-step reaction model:
$C1 \bullet [-\exp(-C2 \bullet t) + \exp(-C3 \bullet t)]$
where $C1$ is a normalized parameter, $C2$ is the lifetime time of one reaction step and $C3$ is lifetime of the other reaction step.

B. The dissociation plot of the red RISC lifetime on the 5B3G target tethered on the glass surface. Data was fitted by the two-step reaction model:
$C1 \bullet [C2 \bullet \exp(-C3 \bullet t) - C3 \bullet \exp(-C2 \bullet t)] / (C2 - C3)$
where $C1$ is a normalized parameter, $C2$ is the lifetime time of one reaction step and $C3$ is lifetime of the other reaction step.

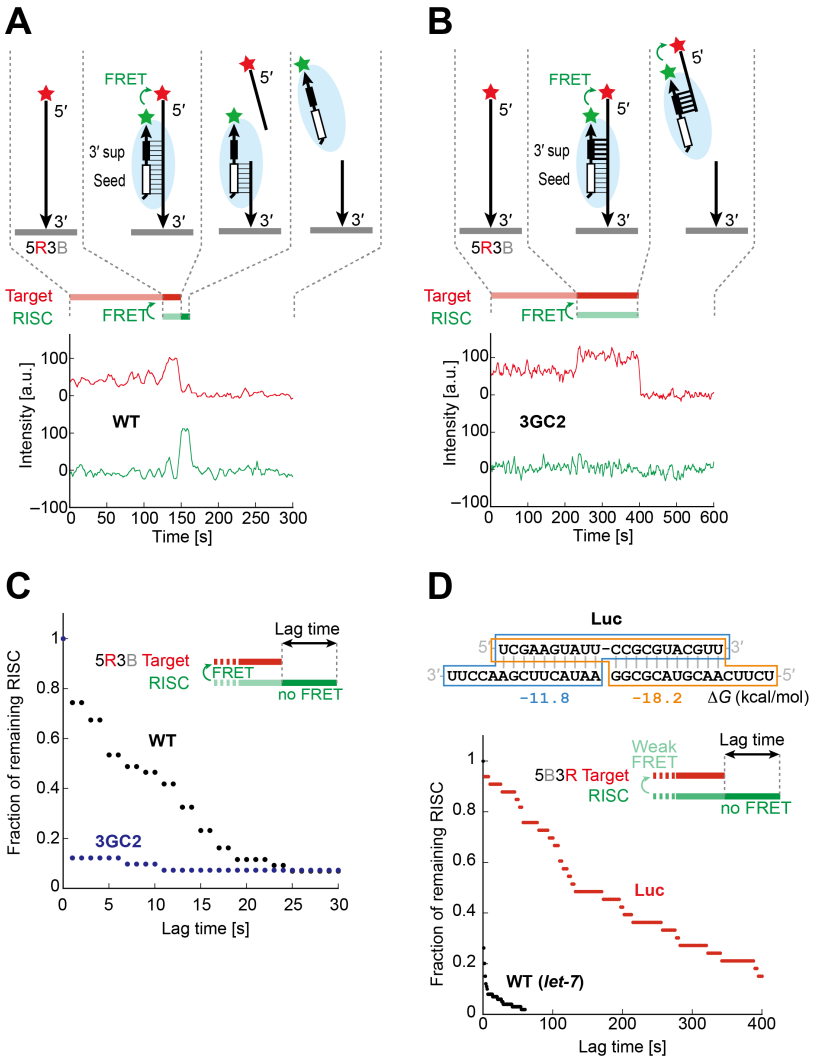

Figure S3. The effect of the guide-target base pairing on the release order of the cleaved target fragments, Related to Figure 3.

A. Continuous single-molecule observation of the cleavage of the WT 5R3B target by green RISC. Note that strong FRET suppresses the green signal and increases the red signal when the red and green spots co-localize.

B. Continuous single-molecule observation of the cleavage of the 3GC2 5R3B target by green RISC. Note that strong FRET suppresses the green signal and increases the red signal when the red and green spots co-localize.

C. Plot of the lag time after the resolution of FRET (i.e., the re-appearance of the green signal) before the disappearance of the green signal in A and B. 3GC2 showed simultaneous departure of the green and red spots (i.e., no re-appearance of the green signal), indicating the prior release of the 3′ cleavage fragment from the seed region.

D. Plot of the lag time after the disappearance of the 5B3R target spots before the disappearance of the green RISC spots. Unlike WT (*let-7*), luc showed a clear lag time, indicating the prior release of the 3′ cleavage fragment from the seed region. The WT (*let-7*) data is the same as in Figure 3E.

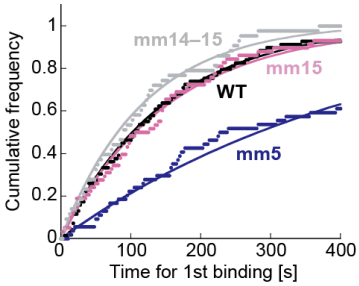

Figure S4. Cumulative plot for the time required for 1st binding, Related to Figure 4.
Calculated time constants (τ) are shown in Figure 4D.